International Immunopharmacology 77 (2019) 105955

Contents lists available at ScienceDirect

International Immunopharmacology

journal homepage: www.elsevier.com/locate/intimp

Activation of RAW264.7 macrophages by active fraction of *Albizia julibrissin* saponin *via* Ca^{2+}–ERK1/2–CREB–lncRNA pathways

Chenying Wang[a], Jing Du[a], Xiangfeng Chen[a], Yongliang Zhu[b], Hongxiang Sun[a,*]

[a] Key Laboratory of Animal Virology of Ministry of Agriculture, College of Animal Sciences, Zhejiang University, Hangzhou, Zhejiang 310058, China
[b] Cancer Institute and Education Ministry Key Laboratory of Cancer Prevention and Intervention, School of Medicine, Zhejiang University, Hangzhou, Zhejiang 310009, China

ARTICLE INFO

Keywords:
Albizia julibrissin
Saponin
Macrophage
Long noncoding RNA (lncRNA)
Microarray
ERK signaling

ABSTRACT

The saponin active fraction from the stem bark of *Albizia julibrissin* (AJSAF) is an ideal vaccine adjuvant, but its mechanism of action remains unclear. The recent evidences indicate that long noncoding RNAs (lncRNAs) play essential roles in regulating the activation and function of macrophages. The current experiments were designed to investigate the effects of AJSAF on the activation of RAW264.7 macrophages and to explore its intracellular molecular mechanisms using a global gene expression microarray. AJSAF could significantly enhance phagocytic activity, induce reactive oxygen species (ROS), promote surface molecule expression, and up-regulate the mRNA and protein expression of cytokines and chemokines in RAW264.7 cells. AJSAF induced the differential expression of 223 mRNAs and 103 lncRNAs in RAW264.7 cells. Bioinformatics were used to predict the potential target mRNAs and function of up-regulated lncRNA A_30_P01018532 in RAW264.7 cells induced by AJSAF. The total 99 co-expressed mRNAs were classified as putative target genes of A_30_P01018532. A_30_P01018532 was associated with the inflammatory and immune response. AJSAF significantly increased the intracellular free Ca^{2+} levels and induced the phosphorylation of ERK1/2 and CREB in RAW264.7 cells. Moreover, Ca^{2+} chelator BAPTA-AM, ERK1/2 inhibitor PD98059 and CREB inhibitor KG-501 significantly inhibited the up-regulation of TNF-α, CCL2, CXCL2, CCL22, and A_30_P01018532 in RAW264.7 cells induced by AJSAF. These results suggested that AJSAF could activate RAW264.7 cells *via* Ca^{2+}–ERK1/2–CREB pathways and that A_30_P01018532 might be an important regulator of mRNA expression in AJSAF-activated macrophage. This study may provide insights into the molecular mechanisms of action of AJSAF.

1. Introduction

Purified recombinant antigens generally elicit weak immune responses unless they are co-formulated with adjuvants. Adjuvants stimulate the innate immune response and shape cellular and humoral responses that eventually confer protection against pathogens [1]. Adjuvants are essential components of new generation vaccines, but still their mechanism of action is poorly understood. The innate immune cells are activated through pattern recognition receptors (PRRs). However, it could hardly explain immune responses to some adjuvants that remarkably activate the immune system but have been identified no PRRs yet. The 'danger' model suggests that immunity might be guided by danger-associated molecular patterns (DAMPs) released from the damaged and dying cells [2,3]. Aluminum compound (Alum) has been shown to have cytotoxic effects resulting in the release of host DNA into the cytoplasm and then influence its adjuvanticity through triggering STING (stimulator of IFN gene)-dependent DNA sensing mechanisms [4,5]. QS-21, a highly characterized adjuvant-active saponin compound isolated from the bark of the *Quillaja saponoria* Molina, induced macrophage and dendritic cell death in a caspase-1-, ASC-, and NLRP3-independent manner at higher concentrations, which might contribute to release of DAMPs resulting in priming a signal and impacting its adjuvant effects [6]. Although the mechanism of action of saponin-based adjuvants is being intensively studied [7–9], it is still not fully elucidated [10].

Long non-coding RNAs (lncRNAs), greater than 200 nucleotides in length, can regulate the mRNA expression in diverse biological contexts [11,12]. Recent evidences indicate that lncRNAs play important roles in directing the development and controlling the activation of macrophages [13]. A series of lncRNAs such as PACER [14], THRIL [15], and lnc-13 [16] in human, as well as lincRNA-Cox2 [17], lincRNA-EPS [18], lncRNA-ACOD1 [19], and lncRNA Mirt2 [20] in mice have been found

* Corresponding author at: College of Animal Sciences, Zhejiang University, Yuhangtang Road 866, Hangzhou 310058, China.
E-mail address: sunhx@zju.edu.cn (H. Sun).

https://doi.org/10.1016/j.intimp.2019.105955
Received 11 June 2019; Received in revised form 7 September 2019; Accepted 30 September 2019
Available online 31 October 2019

to regulate the activation and function of macrophages. The discovery and identification of lncRNAs in the immune cells has provided a new perspective on the gene regulation [21]. Therefore, the study on lncRNAs is likely to reveal the novel mechanism of action of saponin adjuvants.

In our previous studies, the active fraction of saponin from the stem bark of *Albizia julibrissin* Durazz. (AJSAF) has been proved to improve antigen-specific both cellular and humoral immune responses, and simultaneously elicit a Th1/Th2 response in mice to recombinant fowl pox virus vector-based H5 avian influenza vaccine (rFPV) [22] and porcine reproductive and respiratory syndrome virus (PRRSV) vaccine [23], and be a promising adjuvant candidate for vaccine. Many vaccine adjuvants have been reported to act through activating antigen-presenting cells (APCs) such as dendritic cells [24]. Macrophages exert an important role in the immune system as an interface between innate and adaptive immunity [25]. RAW264.7 cells are commonly accepted as a tool to investigate the molecular mechanisms of macrophages involved in regulating immunity [26] and the most suitable model cell lines for dendritic cell [27]. The current experiments were designed to investigate the activation of AJSAF on RAW264.7 macrophages and to explore its intracellular molecular mechanisms, especially the regulation role of lncRNAs using gene expression microarray.

2. Materials and methods

2.1. Reagents

3-(4,5-Dimethylthiazol-2-yl)-2,5-diphenyltetrazolium bromide (MTT), polymyxin B (PMB), fluorescein isothiocyanate-conjugated dextran (FITC-dextran) and KG-501 (CREB inhibitor) were purchased from Sigma Chemical Co., Saint Louis, MO, USA; fetal bovine serum (FBS) was from Gibco, Grand Island, NY, USA; DMEM medium was from Corning, Cellgro, NY, USA; mouse cytokine and chemokine detecting ELISA kits were from Wuhan Boster Biological Technology Co. Ltd., Hubei, China. TRIzol reagent was purchased from Ambion Inc., Carlsbad, CA, USA; revert Aid™ M-MuLV reverse transcriptase was from Fermentas, Amherst, NY, USA; diethylpyrocarbonate (DEPC), ribonuclease inhibitor and oligo$(dT)_{18}$ were from Sangon Biotech (Shanghai) Co., Ltd., China; FastStart universal SYBR Green Master (ROX) was from Roche Diagnostics, Indianapolis, IN, USA. Phycoerythrin (PE)-conjugated anti-mouse CD40 (Clone: 1C10), CD80 (Clone: 16-10A1), CD86 (Clone: PO3.1), MHC-I (H-2 Kb, Clone: AF6-88-5.5.3), and MHC-II (I-Ab, Clone: AF6-120.1) monoclonal antibodies (mAbs) were purchased from eBioscience Inc., San Diego, CA, USA; Fluo-3 AM was from Dojindo Laboratory, Kumamoto, Japan; reactive oxygen species (ROS) assay kit, horseradish peroxidase (HRP)-conjugated goat anti-rabbit and anti-mouse IgG (H + L), enhanced chemiluminescence (ECL) kit and RIPA lysis buffer were from Beyotime Biotech, Jiangsu, China; phosphatase inhibitor cocktail and protease inhibitor cocktail were from Bimake, Houston, TX, USA; anti-mouse actin, IL-1β (D4T2D), anti-rabbit ERK, p-ERK1/2 (Thr202/Tyr204), CREB and p-CREB (Ser133) mAbs were from Cell Signaling Technology, Beverly, MA, USA; Ca^{2+} chelator BAPTA-AM and ERK1/2 inhibitor PD98059 were from Selleck, Houston, TX, USA. SurePrint G3 8 × 60 K mouse gene expression microarray was provided from Agilent Technologies. Santa Clara, CA, USA.

2.2. Preparation and characterization of AJSAF

AJSAF was prepared and characterized as previously described [23]. A total of 29 saponins including 10 new compounds in AJSAF were identified and characterized by high-performance liquid chromatography coupled with quadrupole time-of-flight mass spectrometry based on accurate mass database [28].

2.3. Cell culture

RAW264.7 cells were purchased from the cell bank of the Shanghai Branch of the Chinese Academy of Sciences (Shanghai, China), and maintained in a 5% CO_2 atmosphere in DMEM medium supplemented with 10% FBS, 100 μg/ml streptomycin, and 100 U/ml penicillin.

2.4. Cell viability assay

RAW264.7 cells were seeded at 2×10^4 cell/well in a 96-well plate and incubated at 37 °C in a humidified atmosphere with 5% CO_2. After 24 h, the various concentrations of AJSAF were added into each well and these cells were incubated at 37 °C. 4 h before the end, the cell proliferation was detected using MTT assay as previously described [29].

2.5. Enzyme-linked immunosorbent assay (ELISA)

RAW264.7 cells were incubated with AJSAF (200 μg/ml) for up to 16 h or AJSAF (100, 200, and 250 μg/ml) for 16 h, and the culture supernatant was collected for the detection of TNF-α, CCL2, CXCL2, and CCL22 levels using commercial ELISA kits [29].

2.6. Determination of phagocytic uptake

RAW264.7 cells were treated with AJSAF for 24 h. The cells were harvested and then resuspended in 100 μl FITC-dextran solution (1 mg/ml). After incubation at 37 °C for 30 min, the phagocytic activity was measured using BD FACSVerse System (BD Biosciences, San Jose, CA, USA) [29].

2.7. Surface molecule expression analysis

The surface molecule expression on RAW264.7 cells was determined by flow cytometry [30]. RAW264.7 cells treated with AJSAF for 24 h were harvested and washed with ice-cold PBS containing 2% FCS. Cells were blocked with purified anti-mouse CD16/CD32 antibody (FcR block) for 10 min, and then stained with optimal concentrations of PE-conjugated anti-mouse CD40, CD80, CD86, MHC-I, and MHC-II antibodies for an additional 30 min. The stained cells were analyzed on BD FACSVerse System.

2.8. ROS detection

The intracellular ROS levels were detected using assay kit. After treatment of AJSAF for 2 h, RAW264.7 cells were incubated with 20 μM of 2′,7′-dichlorofluorescin diacetate (DCFH-DA) at 37 °C for 20 min, and then washed with DMEM three times. The mean fluorescence intensity (MFI) was determined by flow cytometry with BD FACSVerse system.

2.9. Intracellular free calcium detection

The intracellular free Ca^{2+} levels were measured by flow cytometry using a fluorescent dye Fluo-3 AM. After exposed to AJSAF at 200 μg/ml for different time, RAW264.7 cells were incubated with 5 μM of Fluo-3 AM at 37 °C for 30 min away from light. The harvested cells were washed twice with HBSS, and then detected for the MFI using flow cytometer at the excitation wave length of 488 nm [31].

2.10. Quantitative real-time PCR (qRT-PCR)

After incubation with or without AJSAF, RAW264.7 cells were subjected to TRIzol reagent. The total RNA was isolated and reverse transcription was performed as previously [32]. The PCR was performed on an ABI 7500 PCR system using FastStart Universal SYBR Green Master (Rox). The PCR cycling was performed as follows: initial denaturation at 95 °C for 10 min followed by 40 cycles of denaturation at 95 °C for 10 s, and annealing at 60 °C for 1 min. The specific primers for qRT-PCR were synthesized by Sangon Biotech (Shanghai) Co., Ltd.

(China) and the sequences were listed in Supplementary Table 1. Primer amplification efficiency and specificity were verified for each set of primers. GAPDH was used as an endogenous control. The mRNA expression levels of the tested genes relative to GAPDH were determined using the $2^{-\Delta\Delta Ct}$ method and shown as fold induction.

2.11. Microarray analysis

Total RNA from RAW264.7 cells was further purified with RNeasy® Mini kit (Qiagen). Fluorescent complementary RNA (cRNA) was generated by Agilent's Low Input Quick Amp Labeling Kit and purified with RNeasy® Mini kit. The integrity of the input template RNA and labeled cRNA was determined using the NanoDrop UV-VIS spectrophotometer and the Agilent 2100 bioanalyzer using RNA 6000 Nano LabChip kit. RNA labelling and hybridization were performed according to the manufacture's protocol. Hybridized microarrays were scanned with Agilent C scanner using Agilent's Scan Control software, version A.8.4.1. The features were extracted with the Feature Extraction software. Data pre-processing and differential expression analysis were done in R software. The data were normalized using the quantile method (GENESPRING12.0). Normalized expression data were subjected to $\log_2$ transformation. P-value < 0.05 and fold change threshold (absolute ratio) > 2 were considered as significant difference [33].

2.12. Functional analysis of differentially expressed mRNAs

Gene Ontology (GO) and Kyoto Encyclopedia of Genes and Genomes (KEGG) analyses were performed for the functions and pathways of differentially expressed mRNAs (DEGs) using DAVID Bioinformatics Resources (version 6.8, https://david.ncifcrf.gov/tools.jsp)[34]. The significance was determined using the Fisher's exact test and χ^2 test, and the threshold of significance was defined by P-value and false discovery rate (FDR). The common and unique ones of KEGG category-associated genes were analyzed by Venn diagram. Ingenuity Pathways Analysis (IPA) software (Ingenuity Systems, Redwood City, CA) was used for network analysis and upstream analysis of DEGs to show crucial effectors and regulatory factors [35].

2.13. Annotation and functional analysis of differentially expressed lncRNAs

Differentially expressed lncRNAs were annotated through the database of Refseq, Ensembl, fRNAdb, and NONCODE [36,37]. The coding potential of each lncRNA was evaluated by using the Coding Potential Calculator (http://cpc.cbi.pku.edu.cn/) [38]. The interaction between transcription factors and lncRNA promoter regions was predicted by omiXcore (http://service.tartaglialab.com/grant_submission/omixcore) [39]. RNAfold web server (http://rna.tbi.univie.ac.at/cgi-bin/RNAWebSuite/RNAfold.cgi) was applied for predicting secondary structures of lncRNA sequences. The co-expressed mRNAs of lncRNAs were identified by Pearson's correlation coefficients between each lncRNA/mRNA pair [40]. The significance was determined using the following cutoff: a Pearson's correlation coefficient > 0.8 or < -0.8 and $P < 0.01$. Next, *cis* and *trans* regulation predictions were performed. In cis-acting analysis, the positions of lncRNAs were searched within 100 kb of their co-expressed mRNAs using the RefSeq and UCSC Known Genes databases (mm10) [41]. Three prediction principles including RNA-RNA, RNA-DNA and RNA-protein interactions were used for the trans-acting analysis. LncRNATargets (http://www.herbbol.org:8001/lrt/) was used to predict the RNA-RNA and RNA-DNA interaction based on nucleic acid thermodynamics [42]. The interaction of lncRNA and RNA-binding protein (RBP) was predicted using RBPDB (The database of RNA-binding protein specificities) [43] and the RBP-binding mRNAs in GO terms were considered as the possible targets of lncRNAs. The interaction networks of lncRNA and its target mRNAs were constructed using Cytoscape [44]. The function of lncRNA was predicted using GO and KEGG analysis based on its target mRNAs.

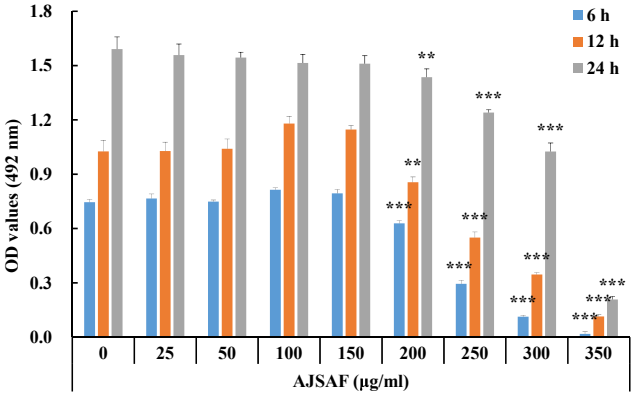

Fig. 1. Effects of AJSAF on the growth of RAW264.7 cells. RAW264.7 cells were treated with AJSAF at the various concentrations for 6, 12 and 24 h, and then cell proliferation was detected using MTT assay. The values are presented as mean ± SD ($n = 4$). Significant differences with control cells (0 μg/ml) were designated as $^{**}P < 0.01$ and $^{***}P < 0.001$.

2.14. Fractionation of nuclear and cytosolic RNA

Fractionation of nuclear and cytosolic RNA was performed as previously described [45]. Briefly, RAW264.7 cells (5×10^6) were harvested and resuspended in 200 μl ice-cold lysis buffer (0.1% NP-40 in PBS) with protease inhibitor cocktail (Bimake) and ribonucleoside vanadyl complex (10 mM) (New England BioLabs) for 2 min on ice. The samples were centrifuged at 12,000 rpm for 5 min at 4 °C. The supernatants containing the cytosolic fraction were mixed with 5 volumes of TRIzol reagent. Pellets were washed twice with ice-cold lysis buffer, and nuclei were lysed with 1 ml TRIzol reagent. RNA was extracted according to the user's manual.

2.15. Western blotting

After treated with AJSAF for various time, RAW264.7 cells were washed twice with cold PBS and lysed with RIPA lysis buffer. The contents of protein were measured with the BCA protein assay kit using bovine serum albumin as a standard. The denatured proteins were separated on 10%–12% SDS-PAGE and transferred to PVDF membrane. After blocking the membrane with 5% skim milk in Tris buffered saline containing 0.1% Tween-20 (TTBS) for 1 h at 37 °C, the blot was incubated with anti-mouse actin, IL-1β, anti-rabbit ERK1/2, p-ERK1/2, CREB, or p-CREB mAbs overnight at 4 °C. Subsequently, the membranes were washed with TTBS and incubated with HRP-conjugated goat anti-mouse or anti-rabbit IgG (H + L) for 1 h. After washing the membrane with TTBS three times, the signal was visualized with ECL on the LiCor C-DiGit Blot scanner (LiCor, Lincoln, NE) [33].

2.16. Inhibition assay

After incubation with BAPTA-AM (25 μM), PD98059 (15 μM) for 0.5 h, or KG-501 (10 μM) for 1 h, RAW264.7 cells were stimulated with AJSAF (200 μg/ml) for 2, 4, or 24 h. The cells and supernatants were collected for detecting the gene expression and protein levels of TNF-α, CCL2, CXCL2, CCL22, and A_30_P01018532 by qRT-PCR and ELISA, respectively.

2.17. Statistical analysis

Data were expressed as mean ± SD and examined for their statistical significance of difference with ANOVA and a Tukey post-hoc test. P-value less than 0.05 was considered to be statistically significant.

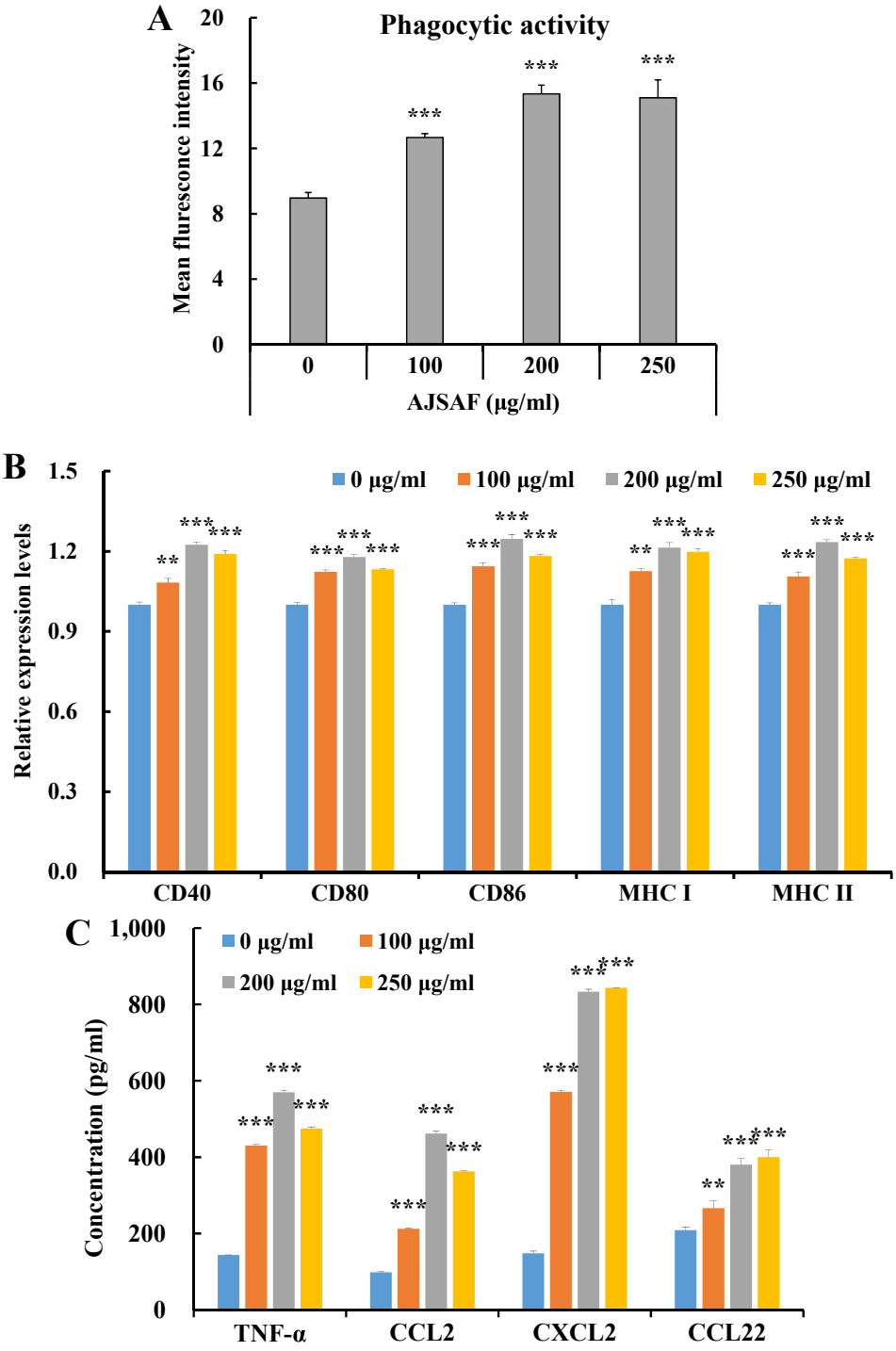

Fig. 2. Effects of AJSAF on the phagocytic activity (**A**), surface molecule expression (**B**), and secretion of cytokines and chemokines (**C**) of RAW264.7 cells. RAW264.7 cells were incubated with AJSAF for 24 h (**A** and **B**) or 16 h (**C**), and then cells and the culture supernatant were collected to measure phagocytic activity, surface molecule expression levels and the contents of TNF-α, CCL2, CXCL2, and CCL22 using flow cytometry and ELISA, respectively. The values are presented as mean ± SD ($n = 3$). Significant differences with 0 μg/ml were designated as $^{**}P < 0.01$ and $^{***}P < 0.001$.

3. Results

3.1. Effects of AJSAF on the growth of RAW264.7 cells

The effects of AJSAF on the growth of RAW264.7 cells were detected using MTT assay, and the results were shown in Fig. 1. AJSAF is not cytotoxic to RAW264.7 cells up to the concentration of 150 μg/ml ($P > 0.05$). However, AJSAF significantly inhibited the proliferation of RAW264.7 cells at the concentration of 200–350 μg/ml in a concentration-dependent manner ($P < 0.001$).

3.2. AJSAF induces the activation of RAW264.7 cells

The effect of AJSAF on phagocytic uptake of FITC-dextran in RAW264.7 cells was examined, and the results were shown in Fig. 2A. AJSAF markedly concentration-dependently promote the phagocytic capacities of macrophages. The expression levels of the accessory and costimulatory molecules on RAW264.7 cells treated with AJSAF for 24 h were

also measured. AJSAF significantly enhanced the expression levels of surface molecules CD40, CD80, CD86, MHC I, and MHC II ($P < 0.01$ and $P < 0.001$, Fig. 2B).

The effects of AJSAF on the production of the cytokines and chemokines from RAW264.7 cells were further detected. As shown in Fig. 2C, AJSAF remarkably concentration-dependently induced the secretion of TNF-α, CCL2, CXCL2, and CCL22 from RAW264.7 cells ($P < 0.001$). AJSAF also significantly concentration-dependently promoted the protein expression of IL-1β (Supplementary Fig. 1) and time-dependently induced the production of TNF-α, CCL2, CXCL2, and CCL22 from RAW264.7 cells (Supplementary Fig. 2).

The mRNA expression levels of cytokines and chemokines in RAW264.7 cells treated with AJSAF at the various concentrations for different times were detected by qRT-PCR. AJSAF remarkably up-regulated the mRNA expression levels of IL-1β, TNF-α, CCL2, CXCL2, and CCL22 in RAW264.7 cells in time- and concentration-dependent manner (Fig. 3).

3.3. Differentially expressed mRNAs and lncRNAs

To clarify the molecular mechanisms of activation of RAW264.7 cell, the cells stimulated with AJSAF (200 μg/ml) for 2 h were subjected to SurePrint G3 8 × 60 K mouse gene expression microarray representing 39,430 mRNA probes and 16,251 lncRNA probes. The work flow of the microarray analysis was shown in Fig. 4. The microarray analysis revealed 394 differentially expressed probes including 270 mRNAs and 124 lncRNAs with FC > 2 and P value ≤ 0.05 compared to untreated samples. Among the differentially expressed probes, 191 mRNA and 47 lncRNA probes were up-regulated, corresponding to 164 and 41 genes, while down-regulated 79 mRNA and 77 lncRNA probes corresponded to 61 and 62 genes, respectively. To confirm the validity of the microarray results, qRT-PCR was undertaken for 12 up-regulated genes (CSF1, CSF3, MARCKS, PTGER2, FLRT3, NLRP3, NOD2, A_30_P01033086, A_30_P01032527, A_30_P01019478, A_30_P01021097, and A_30_P01018532) and 4 down-regulated genes (CASK, MSH4,

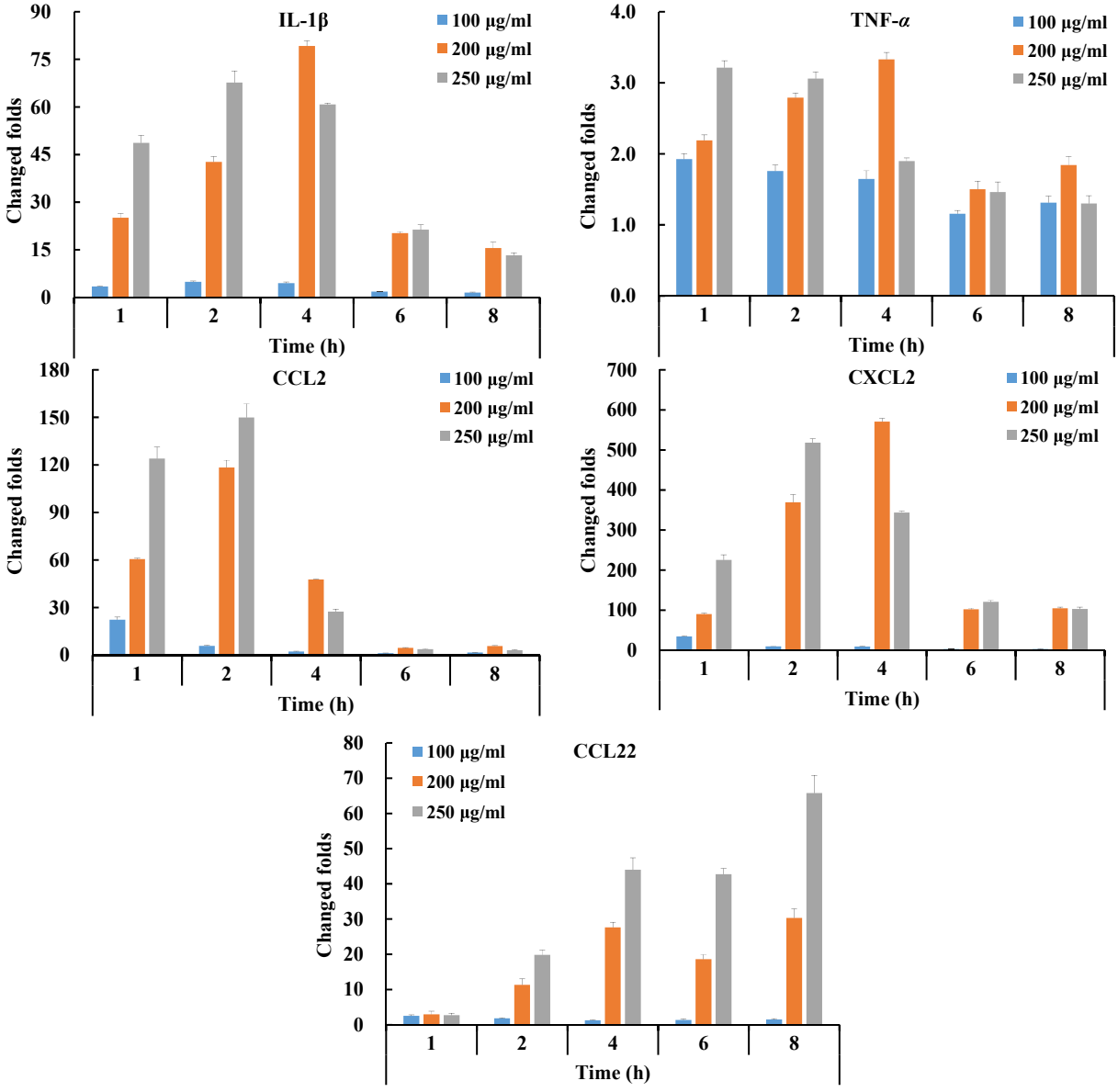

Fig. 3. Effects of the AJSAF on the mRNA expression of cytokines and chemokines in RAW264.7 cells. RAW264.7 were incubated with medium or AJSAF (100, 200, or 250 μg/ml) for up to 8 h, the mRNA expression levels of IL-1β, TNF-α, CCL2, CXCL2, and CCL22 were measured using qRT-PCR. The values are presented as mean ± SD ($n = 3$). Significant differences with control cells (0 μg/ml) were designated as $^{**}P < 0.01$ and $^{***}P < 0.001$.

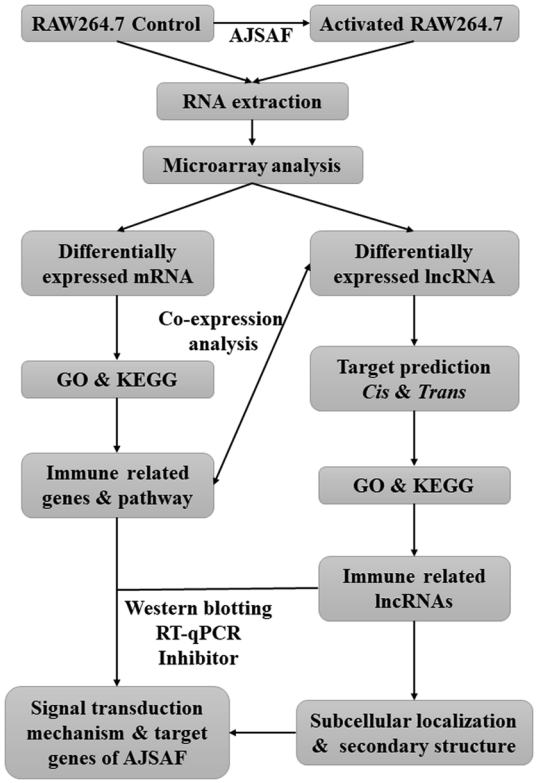

Fig. 4. Work flow of the microarray analysis of RAW264.7 cells treated with AJSAF.

A_30_P01033073, and A_30_P01029853). AJSAF-induced expression levels of selected genes by qRT-PCR were consistent with microarray analysis data (Supplementary Fig. 3). Among DEGs, 38 genes (IL-1α, IL-1β, TNF-α, CXCL2, CCL4, SOCS3, TNFRSF1B, ZC3H12A, INHBA, SAA3, CCRL2, ICOSL, MTMR7, TNFAIP3, NFKBIZ, STX11, KDM6B, ADORA2A, CDC42EP2, ARG2, GPR84, DUSP2, TNFSF9, GADD45B, PPFIA3, FAS, 1200009I06Rik, NIACR1, CLEC4E, JAG1, BCL3, GCH1, JUNB, NFKBIA, A130040M12Rik, ICAM1, CENPP, and CD84) were defined as distinct M1 markers, 20 genes (IL-10, CCL7, CCL24, CD83, CISH, FLRT3, CSF1, HBEGF, AHR, MMP9, IRF4, PTPRE, 4833422F24Rik, SPHK1, MYC, ZBTB46, ERRFI1, REL, 5330406M23Rik, and IFIT2) were as distinct M2 markers, while 20 (PTGER2, OLR1, PDE4B, CCL22, PIM1, IER3, IRG1, CD40, PHLDA1, NFKBIE, MALT1, PTGS2, 3930401B19Rik, TRAF1, SRC, ST3GAL1, JDP2, TCF4, FGD4, and KLHL6) were common to both M1 and M2 macrophages (Supplementary Table 2) based on GSE69607database [46].

3.4. GO and KEGG analysis of differentially expressed mRNAs

All 223 DEGs have been subjected to GO functional analysis, and the results were shown in Fig. 5A. The molecular function included 'cytokine activity' ($P = 7.73 \times 10^{-15}$), 'chemokine activity' ($P = 7.59 \times 10^{-5}$), 'CCR chemokine receptor binding' ($P = 1.18 \times 10^{-4}$), 'protein binding' ($P = 6.10 \times 10^{-4}$), 'TNF receptor binding' ($P = 3.09 \times 10^{-3}$), and 'calmodulin binding' ($P = 2.63 \times 10^{-2}$). The biological process were connected to 'inflammatory response' ($P = 1.94 \times 10^{-20}$), 'immune response' ($P = 1.33 \times 10^{-10}$),' 'cellular response to IL-1' ($P = 4.58 \times 10^{-9}$), 'regulation of ERK1 and ERK2 cascade' ($P = 2.66 \times 10^{-7}$), 'regulation of NF-κB activity' ($P = 1.02 \times 10^{-6}$), and 'neutrophil chemotaxis' ($P = 4.26 \times 10^{-6}$).

KEGG analysis was used to identify the immune-related pathway of the DEGs. The most significant pathways were 'TNF pathway' ($P = 2.79 \times 10^{-16}$), 'cytokine-cytokine receptor interaction' ($P = 4.13 \times 10^{-10}$), 'NF-κB pathway' ($P = 1.89 \times 10^{-7}$), 'Jak-STAT pathway' ($P = 5.24 \times 10^{-5}$), 'NOD-like receptor (NLR) pathway' ($P = 5.10 \times 10^{-4}$), and 'MAPK pathway' ($P = 0.003$) (Fig. 5B). The Venn diagram was generated for clarifying the relationship among the enriched KEGG pathways. There were two 'focus' genes IL-1β and TNF in the terms of 'TNF signaling pathway', 'NF-κB pathway', 'NLR pathway', and 'MAPK pathway' (Fig. 5C). Several gene expressions were unique for each pathway, with BCL3, SOCS3, CSF1, IL15, JUNB, LIF, MMP9, CXCL2, CX3CL1, and TNFRSF1B for 'TNF signaling pathway', LTB, CCL4, CD40, and MALTL for 'NF-κB pathway', NLRP3 for 'NLR pathway', and IL-1α, PDGFB, DUSP2, DUSP5, GADD45A, GADD45B, and MYC for 'MAPK pathway', respectively.

3.5. Core genes and core regulators of differentially expressed mRNAs

To clarify the core genes of DEGs, a 'focus gene' network was generated using IPA software. TNF-α and IL-1β were identified to be two focus genes in the network consisting of 108 genes (Fig. 5D). The upstream analysis revealed that TNF ($z = 4.113$, $P = 8.81 \times 10^{-26}$), IL-1β ($z = 4.344$, $P = 3.73 \times 10^{-18}$), and ERK1/2 ($z = 3.236$, $P = 2.32 \times 10^{-14}$) were the core regulators involved in the immune response of RAW264.7 cells to AJSAF (Fig. 5E). IPA pathway analysis showed that Ca^{2+} pathway activated ERK cascade and its downstream transcription factor CREB in AJSAF-treated RAW264.7 cells (Fig. 5F).

3.6. Annotation and functional prediction of A_30_P01018532

To unveil potential associations between lncRNAs and mRNAs, TOP 10 up-regulated lncRNA probes were subjected to bioinformatic analyses (Supplementary Table 3). A_30_P01027990 and A_30_P01033086 were predicted to possess coding abilities. A_30_P01025400, A_30_P01023376, and A_30_P01017981 were found to have no significant difference between their probe signal and the background. Among the other 5 lncRNA probes (A_30_P01018532, A_30_P01032527, A_30_P01025874, A_30_P01019478, and A_30_P01021097) detected in both control and AJSAF-treated RAW264.7 cells based on microarray analysis, A_30_P01018532 (coding potential score −0.994) was the most up-regulated lncRNA in RAW64.7 cells induced by AJSAF, and selected for annotation and functional analysis.

The prediction of target mRNAs might provide a foundation to analyze the function of lncRNAs. The co-expressed mRNAs were classified as the potential target genes of lncRNA. Firstly, the correlation analysis of A_30_P01018532 and 124 differentially expressed immune-related mRNAs was conducted to afford 104 co-expressed mRNAs. Secondly, two independent algorithms (*cis* and *trans*) were used to predict the potential targets of A_30_P01018532. For the cis-acting analysis, the mRNAs in the same chromosome 100 kb upstream and downstream of A_30_P01018532 were searched, and no target mRNAs were found. Meanwhile, two platforms lncRNA Targets and RBPDB were used to predict the trans-target genes of A_30_P01018532. By analyzing the interaction of A_30_P01018532 with mRNA (lncRNA–RNA) and promoter sequence (lncRNA–DNA) of its co-expressed mRNAs, 20 (Fig. 6A) and 24 (Fig. 6B) mRNAs were predicted to be putative target genes. Through 32 RBPs probably interacting with A_30_P01018532, 90 co-expressed mRNAs were predicted to be putative trans-target genes (Fig. 6C). Collectively, 99 putative target mRNAs of the A_30_P01018532 were obtained after excluding duplicate genes. The GO function analysis of A_30_P01018532 target mRNAs was conducted and the results were shown in Fig. 6D. The main enriched biological processes were the 'inflammatory response' ($P = 1.12 \times 10^{-21}$), 'immune response' ($P = 5.16 \times 10^{-15}$), 'cellular response to IL-1' ($P = 4.27 \times 10^{-10}$), 'regulation of ERK1 and ERK2 cascade' ($P = 5.23 \times 10^{-9}$), 'regulation of NF-κB activity' ($P = 6.91 \times 10^{-9}$), and 'regulation of apoptotic process' ($P = 9.48 \times 10^{-9}$). The enriched molecular functions mainly included the 'cytokine activity' ($P = 2.68 \times 10^{-18}$), 'protein binding' ($P = 3.41 \times 10^{-9}$), 'chemokine activity' ($P = 5.52 \times 10^{-6}$), 'growth factor activity'

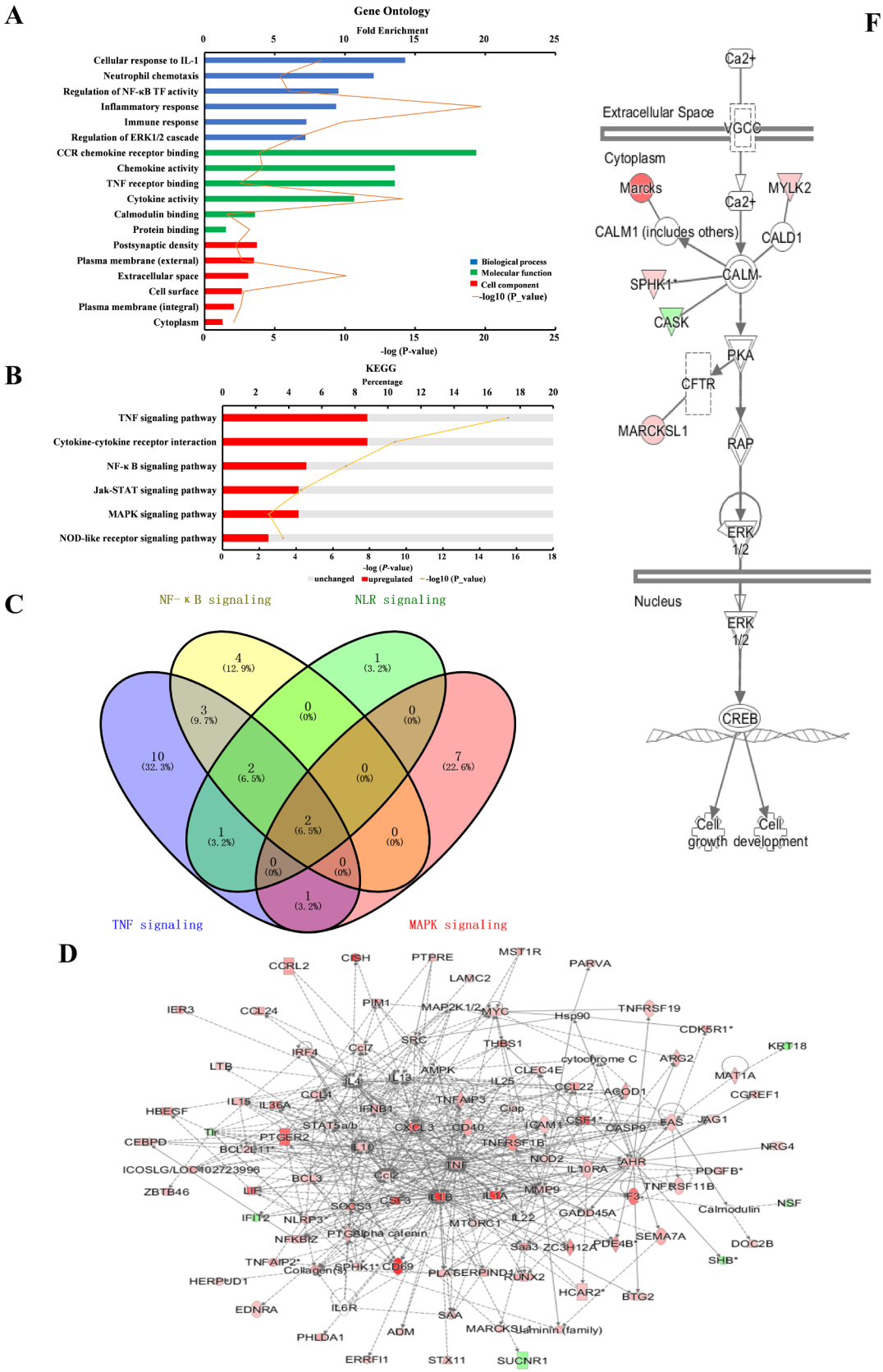

Fig. 5. GO, KEGG and IPA analysis of differentially expressed mRNAs (DEGs) in RAW264.7 cells treated with AJSAF (200 μg/ml) for 2 h. (**A**) GO function. (**B**) KEGG immune-related pathways. (**C**) Venn diagram showing shared and unique DEGs in four pathways. The network analysis (**D**), upstream analysis (**E**) and pathway analysis (**F**) of DEGs using IPA software.

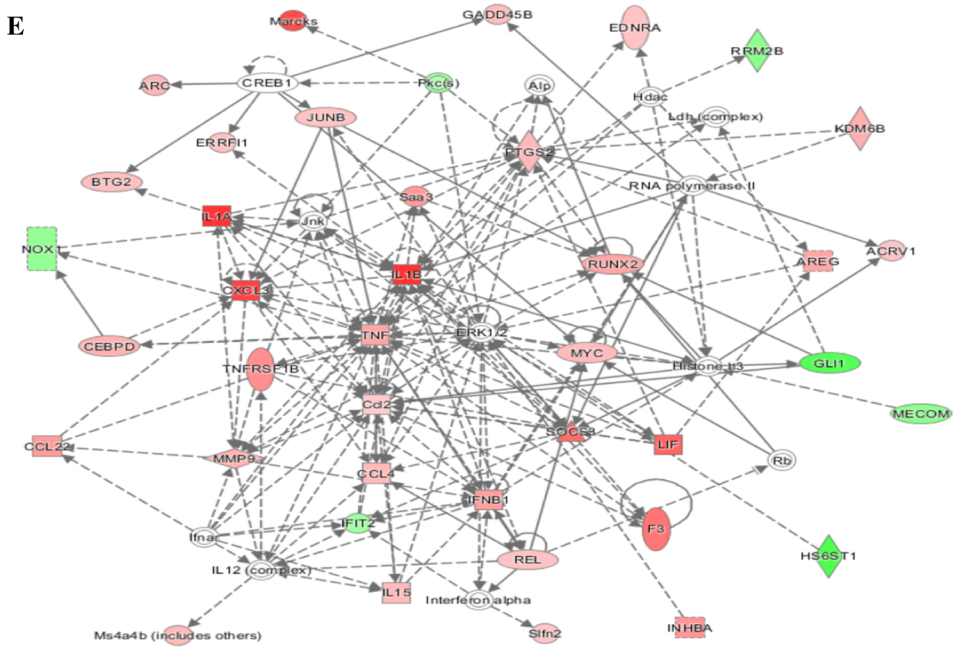

Fig. 5. (*continued*)

($P = 1.24 \times 10^{-5}$), 'TNF-activated receptor activity' ($P = 1.57 \times 10^{-4}$), and 'CCR chemokine receptor binding' ($P = 4.36 \times 10^{-4}$). KEGG analysis indicated that A_30_P01018532 could be involved in 'TNF signaling pathway' ($P = 2.39 \times 10^{-19}$), 'cytokine-cytokine receptor interaction' ($P = 7.04 \times 10^{-12}$), 'NF-κB pathway' ($P = 5.30 \times 10^{-9}$), 'Jak-STAT pathway' ($P = 2.32 \times 10^{-5}$), 'NLR pathway' ($P = 9.22 \times 10^{-5}$), and 'MAPK signaling pathway' ($P = 0.001$) (Fig. 6E).

The orientation and 307 nt sequence of A_30_P01018532 were confirm using RT-PCR. A_30_P01018532 was proved to locate in the nucleus using fractionation of nuclear and cytosolic RNA and PCR (Fig. 6F). A_30_P01018532 was encoded by the opposite strand of the MRLN on chromosome 10 (Fig. 6G). The second structure of A_30_P01018532 possessed RNA binding domain and several RBP binding motifs, including the sequence that could combine with MRLN's third exon (Fig. 6H).

3.7. Ca^{2+}–ERK1/2–CREB pathway was essential for activation of RAW264.7 cells by AJSAF

The effects of AJSAF on intracellular ROS generation in RAW264.7 cells were determined. As shown in Fig. 7A, AJSAF significantly concentration-dependently induced production of ROS from RAW264.7 cells ($P < 0.001$). AJSAF also increased intracellular free calcium levels in a time- and concentration-dependent manner (Fig. 7B). Moreover, Ca^{2+} chelator BAPTA-AM remarkably suppressed the up-regulated expression levels of TNF-α, CCL2, CXCL2, CCL22, and A_30_P01018532 (Fig. 7C) as well as the secretion of TNF-α, CCL2, CXCL2, and CCL22 in RAW264.7 cells induced by AJSAF (Fig. 7D). These results revealed that Ca^{2+} signaling was involved in AJSAF-mediated RAW264.7 cell activation.

IPA analysis suggested ERK as one of the possible upstream molecules involved in the activation of RAW264.7 cells induced by AJSAF (Fig. 5E). Meanwhile, omiXcore predicted that the downstream transcription factor CERB of ERK1/2 could bind to the promoter region A_30_P01018532 with the score 0.97 (Supplementary Fig. 4). To investigate whether AJSAF activated RAW264.7 cells *via* this pathway, the phosphorylation of ERK1/2 and CERB in RAW264.7 cells were detected by western blotting. AJSAF significantly induced the phosphorylation of ERK1/2 and CREB from 15 min to 120 min (Fig. 7E). Pretreatment with ERK1/2 inhibitor PD98059 and CREB inhibitor KG-501 significantly inhibited the up-regulated expression levels of TNF-α, CCL2, CXCL2, CCL22, and A_30_P01018532 in RAW264.7 cells induced by AJSAF (Fig. 7F–G). Collectively, these results confirmed the involvement of ERK1/2-CREB in the activation of RAW264.7 cells induced by AJSAF.

4. Discussion

AJSAF has been previously reported to exert the immunological adjuvant effects on rFPV [22] and PRRSV vaccine [23] by inducing cytokine and chemokine immunostimulatory environment at the site of injection. However, its further mechanism of action is to be addressed. Many vaccine adjuvants were proved to act through activating macrophages [24]. In the present study, AJSAF was investigated for the potential to activate RAW264.7 macrophages and its intracellular molecular mechanisms.

AJSAF significantly promoted the phagocytic capacity and the expression of the surface molecules CD40, CD80, CD86, MHC I, and MHC II. AJSAF could markedly time- and concentration-dependently not only induced the release of cytokines (IL-1β and TNF-α) and chemokines (CCL2, CXCL2 and CCL22) from RAW264.7 cells, but up-regulated the mRNA expression levels of IL-1β, TNF-α, CCL2, CXCL2, and CCL22 in RAW264.7 cells. Damaged and dead cells produce and release small endogenous DAMPs, which activate innate immune cells and initiate adaptive immune response [2]. The role of DAMPs, such as uric acid [47], DNA [3,5], and ATP [48] in adjuvant effects of Alum and MF59 has been confirmed. In view of that AJSAF was cytotoxic to RAW264.7 at the concentration > 150 μg/ml, the activation of macrophages induced by AJSAF might contribute to its limited cytotoxicity resulting in release of DAMPs.

To investigate the molecular mechanisms associated with AJSAF-induced macrophage activation, the gene expression microarray was performed for AJSAF-treated RAW264.7 cells. AJSAF induced the differential expression of 223 annotated mRNAs and 103 non-redundant lncRNAs in RAW264.7 cells. Among the DEGs, the mRNA expression levels of 38 distinct M1, 20 typical M2, and 20 markers common to both M1 and M2 in RAW264.7 cells were up-regulated by AJSAF, suggesting that AJSAF elicited both M1 and M2 polarization of macrophages. These results further confirmed that AJSAF could induce the activation

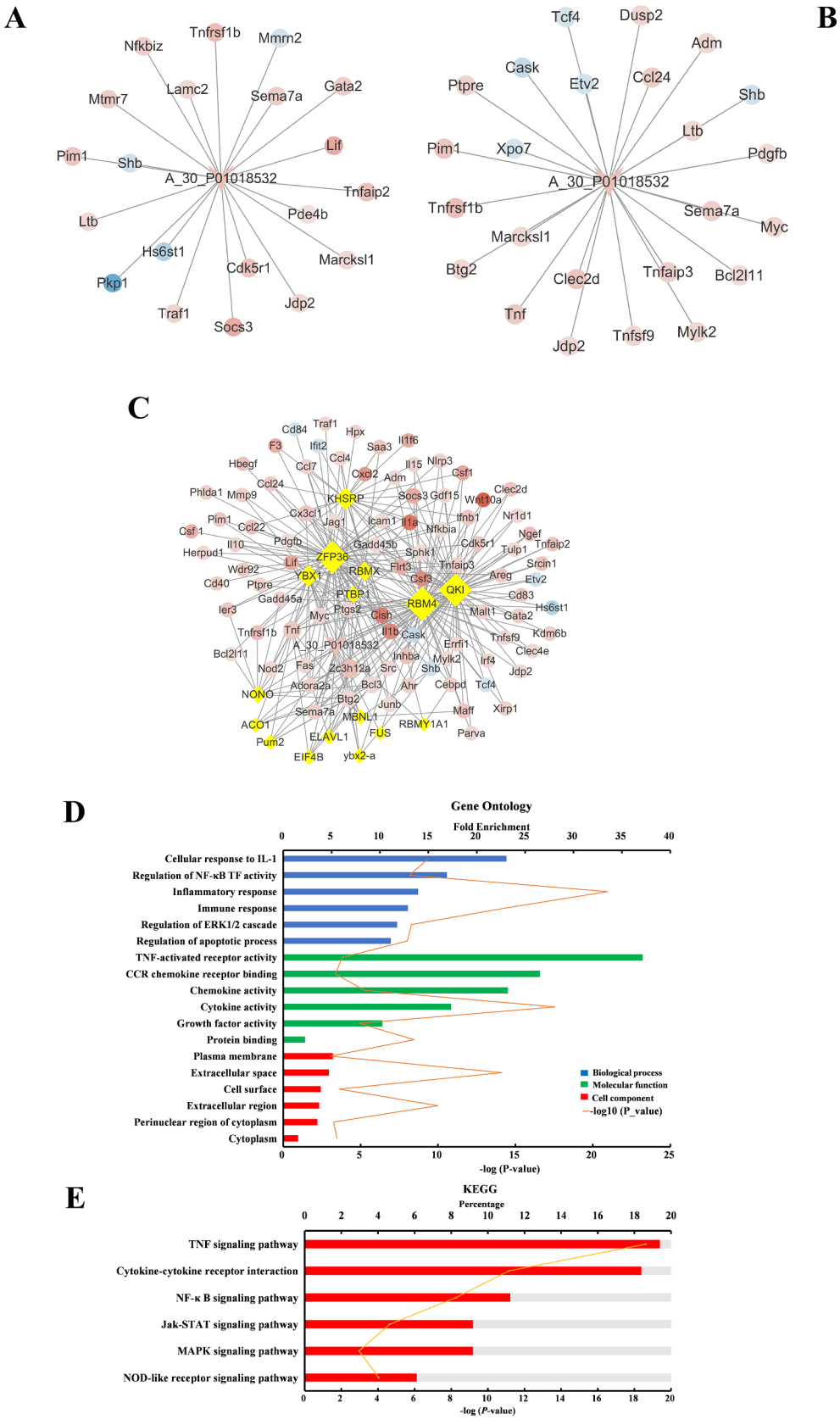

Fig. 6. Annotation and functional prediction of A_30_P01018532. The potential target mRNAs of A_30_P01018532 by predicting the interaction with mRNA (**A**), DNA (**B**), and RBP (**C**). GO (**D**) and KEGG (**E**) analysis of A_30_P01018532 potential target mRNAs. (**F**) Location of A_30_P01018532 in RAW264.7 cells. (**G**) Annotation of A_30_P01018532. (**H**) Centroid secondary structure of A_30_P01018532 with the RNA binding domain and RBP binding motif.

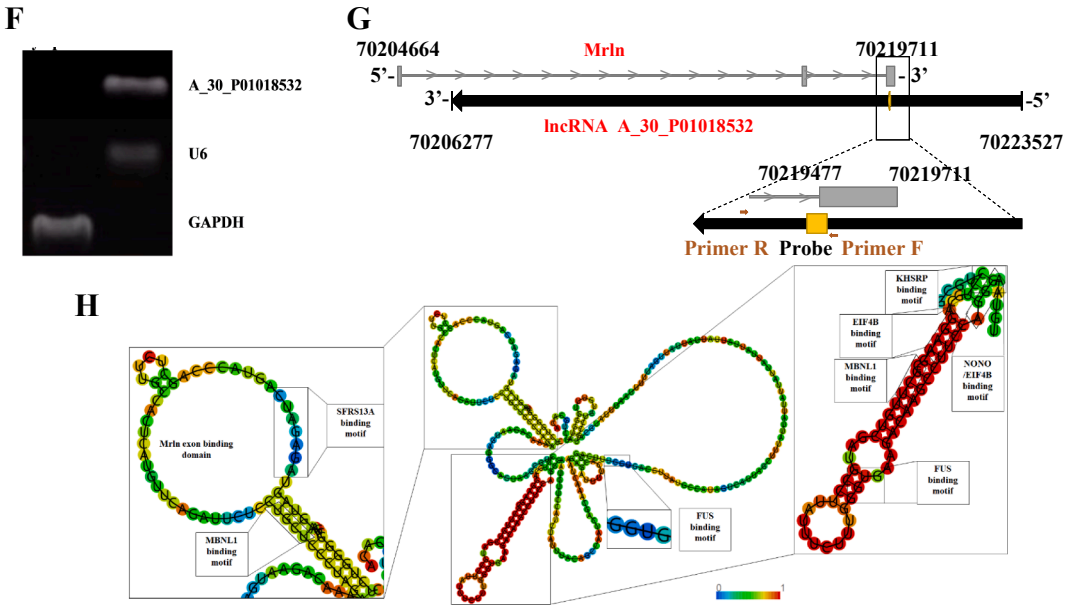

Fig. 6. (*continued*)

of macrophage and were consistent with that AJSAF elicited a balanced Th1/Th2 response to rFPV [22] and PRRSV vaccine [23].

Using KEGG analysis, 'TNF signaling pathway', 'NF-κB pathway', 'NLR pathway', and 'MAPK pathway' were identified as the main immune-related pathways of the DEGs in RAW264.7 cells induced by AJSAF. All four pathways contained 2 common genes IL-1β and TNF. Furthermore, IL-1β and TNF were also identified as the core genes in the network of immune-related DEGs in AJSAF-activated RAW264.7 cells. TNF-α was reported to be a key mediator of the interaction between macrophages and epithelial cells necessary for induction of cytokine responses [49]. The upstream analysis identified TNF, IL-1β and ERK1/2 as core regulators in AJSAF-activated RAW264.7 cells. IPA pathway analysis revealed that AJSAF activated ERK cascade and its downstream CREB in RAW264.7 cells *via* Ca^{2+} pathway.

LncRNAs are important regulators of mRNA expression and achieve regulatory specificity through interacting with RNA, DNA, and RBPs [50–52]. In this study, the microarray analysis revealed that AJSAF induced 103 differentially expressed lncRNAs in RAW264.7 cells. Based on the protein-coding potential, evolutionary conservation, and qRT-PCR verification, A_30_P01018532 was selected for further annotation and functional prediction. Three putative regulatory models such as RNA–RNA, RNA–DNA, and RNA–protein interactions were employed to predict the target gene of A_30_P01018532. Among 104 co-expressed mRNAs, 99 were identified as potential target genes of A_30_P01018532. GO analysis of these putative target mRNAs revealed that A_30_P01018532 involved in 'inflammatory response', 'immune response', 'cellular response to IL-1', 'regulation of ERK1 and ERK2 cascade', 'regulation of NF-κB activity', and 'regulation of apoptotic process'. The KEGG pathway analysis indicated that 'TNF signaling pathway', 'cytokine-cytokine receptor interaction', 'NF-κB pathway', and 'Jak-STAT pathway' involved in activation of RAW264.7 cells induced by AJSAF. These results were consistent with functional characterization of AJSAF-activated macrophages, suggesting the core regulatory roles of A_30_P01018532 in macrophage activation by AJSAF.

Because of its location in the nucleus, A_30_P01018532 could regulate the transcription of target mRNAs *via* base-pair interactions. MRLN (2310015B20Rik) exon 3 could bind with A_30_P01018532. MRLN was reported to involve in the regulation of Ca^{2+} uptake into the sarcoplasmic reticulum [53]. RNA–DNA interaction analysis revealed that A_30_P01018532 could form duplex base-pairing interactions with the promoter of 24 DEGs such as TNF, CLEC2D, calcium/calmodulin-dependent serine protein kinase (CASK), and myristoylated alanine rich protein C substrate-like 1 (MARCKSL1). It was reported that CASK interacted with Ca^{2+} pump 4b/CI [54] and MARCKSL1 had a very strong affinity for calcium-bound calmodulin [55,56]. Therefore, it was speculated that A_30_P01018532 might be a regulator in AJSAF-induced Ca^{2+} signaling. We also performed RNA–protein interaction prediction to figure out 32 RBPs, which involved in the transcription of 90 target genes. A_30_P01018532 contained the motifs bound to ZFP36, KHSRP, EIF4B, MBNAL, and FUS, which formed a stable long stem of the secondary structure. ZFP36 and KHSRP were at the center of A_30_P01018532–RBP–mRNA networks. ZFP36 was reported to regulate CREB activity [57] and bind to the A + U-rich element in the TNF-α 3′-untranslated region which promoted deadenylation and destabilization of the TNF-α mRNA [58]. KHSRP is an important regulator of pro-inflammatory genes TNF-α, IL-8, and iNOS [59]. Therefore, A_30_P01018532 could mediate AJSAF-induced activation of RAW264.7 cells through interacting with ZFP36 and KHSRP.

AJSAF induced the generation of ROS in RAW264.7 cells. ROS exert positive or negative modulation on the activity of different calcium channels. GO molecular function analysis of DEGs in RAW264.7 cells induced by AJSAF identified MARCKS, MYH3, SPHK1, MARCKSL1, and MYLK2 enriched in 'calmodulin binding'. In this study, AJSAF induced a sustained intracellular Ca^{2+} rise in RAW264.7 cells. Moreover, Ca^{2+} chelator BAPTA-AM significantly reduced AJSAF-induced expression of TNF-α, CCL2, CXCL2, CCL22, and A_30_P01018532. These results suggested that Ca^{2+} pathway was involved in AJSAF-mediated macrophage activation.

Ca^{2+} signal induced the phosphorylation of ERK1/2 and CREB [60,61]. GO biological process and KEGG analysis of the DEGs in RAW264.7 cells induced by AJSAF revealed that ERK1/2 cascade was involved in AJSAF-mediated molecular mechanism. The upstream analysis also identified ERK1/2 as a core upstream regulator in AJSAF-activated RAW264.7 cells, regulating DEGs such as SOCS3, MYC, IL-1β, CXCL2, TNF, CCL2, MMP9, CCL4, and SAA3. Minutes after AJSAF treatment, the expression levels of ERK1/2 and CREB phosphorylation were up-regulated. AJSAF-induced TNF-α, CCL2, CXCL2, CCL22, and A_30_P01018532 expression levels in RAW264.7 cells were also significantly suppressed by ERK1/2 inhibitor (PD98059) and CREB inhibitor (KG-501). Thus, AJSAF-induced intracellular Ca^{2+} could promote the phosphorylation of ERK1/2 and CREB resulting in the activation of macrophages.

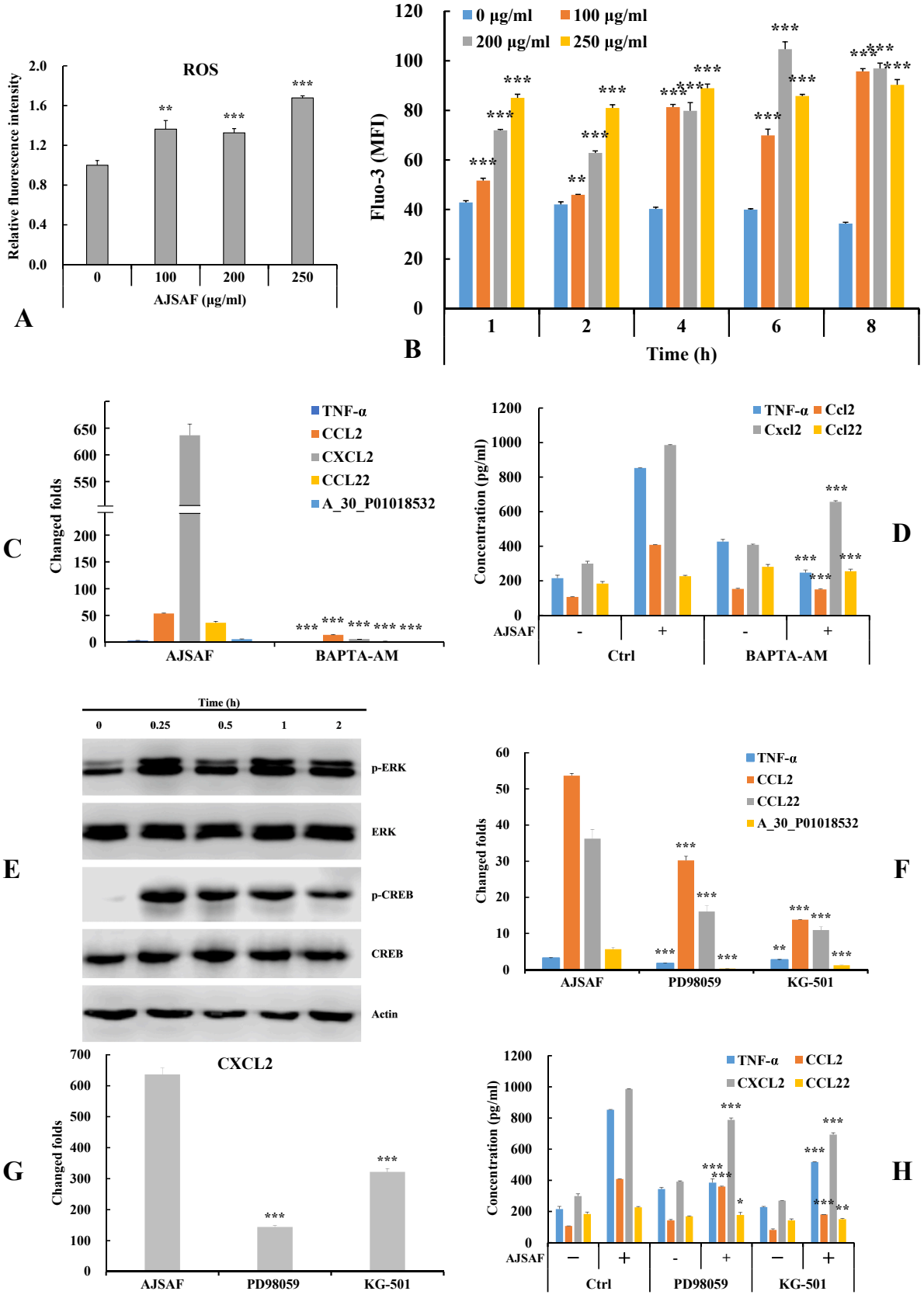

(caption on next page)

Fig. 7. Roles of Ca^{2+}–ERK1/2–CREB pathway in activation of RAW264.7 cells by AJSAF. (**A** and **B**) RAW264.7 cells were incubated with medium or AJSAF (150, 200, or 250 μg/ml), and then collected to detect the levels of ROS (**A**, 2 h) and intracellular free calcium (**B**, 1–8 h). (**C** and **D**) After pre-incubation with or without BAPTA-AM (25 μM) for 30 min, RAW264.7 cells were treated with AJSAF (200 μg/ml) for 2 or 24 h, and then the gene expression levels (**C**, 2 h) and the contents in the culture supernatants (**D**, 24 h) of TNF-α, CCL22, CXCL2, CCL22, and A_30_P01018532 were detected by qRT-PCR and ELISA, respectively. (**E**) RAW264.7 cells were treated with AJSAF (200 μg/ml) for 0, 15, 30, 60, and 120 min, the protein levels were detected by Western blotting. The figure shown is representative of three independent experiments. (**F–H**) After pre-incubation with or without PD98059 for 30 min or KG-501 for 1 h, RAW264.7 cells were treated with medium or AJSAF (200 μg/ml) for 2 or 24 h, and then the gene expression levels (**F** and **G**, 2 h) and the contents in the culture supernatants (H, 24 h) of TNF-α, CCL2, CXCL2, CCL22, and A_30_P01018532 were detected by qRT-PCR and ELISA, respectively. The values are presented as mean ± SD ($n = 3$). Significant differences with control cells (0 μg/ml) were designated as $^{*}P < 0.05$, $^{**}P < 0.01$ and $^{***}P < 0.001$.

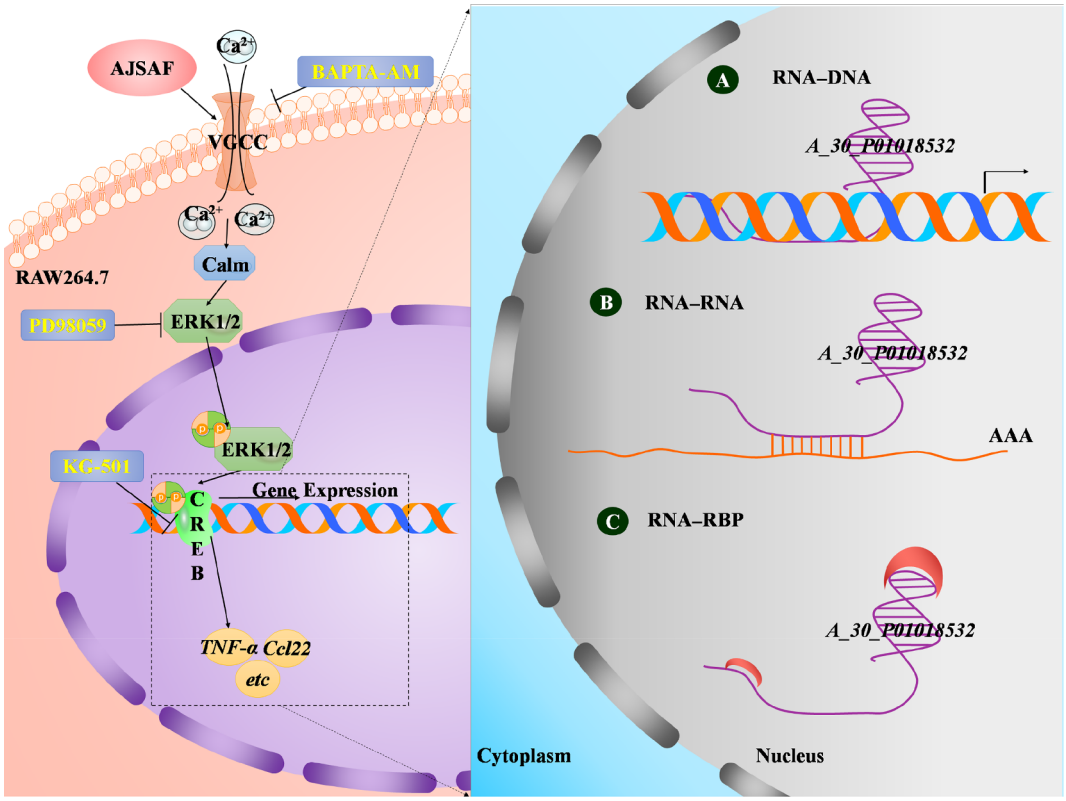

Fig. 8. Possible mechanisms in activation of RAW264.7 cells induced by AJSAF and action mode of A_30_P01018532. AJSAF activates RAW264.7 cells *via* Ca^{2+}–ERK1/2–CREB pathway resulting in up-regulation of the mRNA expression of cytokine and chemokines. A_30_P01018532 might participate in Ca^{2+}–ERK1/2–CREB pathway by regulating its target gene through interaction with DNA (**A**), mRNA (**B**), or RBP (**C**).

In conclusion, we first investigated the expression profile of mRNAs and lncRNAs in RAW264.7 cells activated by AJSAF. Secondly, our experimental data revealed AJSAF could activate RAW264.7 cells *via* Ca^{2+}–ERK1/2–CREB signaling. Furthermore, A_30_P01018532 was predicted to participate in Ca^{2+}–ERK1/2–CREB pathway by regulating its target mRNAs through interaction with DNA, mRNA like MRLN or RBP like KHSRP (Fig. 8). This study might provide insights into the molecular mechanisms of action of AJSAF. Further studies are still required to elucidate the biological functions of *A_30_P01018532* and its mechanisms.

Acknowledgments

This work was supported by Grant-in-Aid from the National Key R& D Program of China (2017YFD0501505), the National Natural Science Foundation of China (Nos. 31272597, 31472229, and 31772783), the Zhejiang Provincial Natural Science Foundation of China (No. LZ13C180001), and the Dabeinong Funds for Discipline Development and Talent Training in Zhejiang University.

Declaration of Competing interests

The authors declare no competing interests.

Appendix A. Supplementary material

Supplementary data to this article can be found online at https://doi.org/10.1016/j.intimp.2019.105955.

References

[1] S.G. Reed, M.T. Orr, C.B. Fox, Key roles of adjuvants in modern vaccines, Nat. Med. 19 (2013) 1597–1608.
[2] G.P. Amarante-Mendes, S. Adjemian, L.M. Branco, L.C. Zanetti, R. Weinlich, K.R. Bortoluci, Pattern recognition receptors and the host cell death molecular machinery, Front. Immunol. 9 (2018) 2379, https://doi.org/10.3389/fimmu.2018.02379.
[3] S.P.M. Sok, D. Ori, N.H. Nagoor, T. Kawai, Sensing self and non-self DNA by innate immune receptors and their signaling pathways, Crit. Rev. Immunol. 38 (2018) 279–301.
[4] A.S. McKee, M.A. Burchill, M.W. Munks, L. Jin, J.W. Kappler, R.S. Friedman, J. Jacobelli, P. Marrack, Host DNA released in response to aluminum adjuvant

enhances MHC class II-mediated antigen presentation and prolongs CD4 T-cell interactions with dendritic cells, Proc. Natl. Acad. Sci. U. S. A. 110 (2013) E1122–E1131.
[5] T. Marichal, K. Ohata, D. Bedoret, C. Mesnil, C. Sabatel, K. Kobiyama, P. Lekeux, C. Coban, S. Akira, K.J. Ishii, F. Bureau, C.J. Desmet, DNA released from dying host cells mediates aluminum adjuvant activity, Nat. Med. 17 (2011) 996–1002.
[6] R. Marty-Roix, G.I. Vladimer, K. Pouliot, D. Weng, R. Buglione-Corbett, K. West, J.D. MacMicking, J.D. Chee, S. Wang, S. Lu, E. Lien, Identification of QS-21 as an inflammasome-activating molecular component of saponin adjuvants, J. Biol. Chem. 291 (2016) 1123–1136.
[7] S.P. Cibulski, M. Rivera-Patron, G. Mourglia-Ettlin, C. Casaravilla, A.C.A. Yendo, A.G. Fett-Neto, J.A. Chabalgoity, M. Moreno, P.M. Roehe, F. Silveira, *Quillaja brasiliensis* saponin-based nanoparticulate adjuvants are capable of triggering early immune responses, Sci. Rep. 8 (2018) 13582, https://doi.org/10.1038/s41598-018-31995-1.
[8] M.H. den Brok, C. Büll, M. Wassink, A.M. de Graaf, J.A. Wagenaars, M. Minderman, M. Thakur, S. Amigorena, E.O. Rijke, C.C. Schrier, G.J. Adema, Saponin-based adjuvants induce cross-presentation in dendritic cells by intracellular lipid body formation, Nat. Commun. 7 (2016) 13324, https://doi.org/10.1038/ncomms13324.
[9] I. Welsby, S. Detienne, F. N'Kuli, S. Thomas, S. Wouters, V. Bechtold, D. De Wit, R. Gineste, T. Reinheckel, A. Elouahabi, P.J. Courtoy, A.M. Didierlaurent, S. Goriely, Lysosome-dependent activation of human dendritic cells by the vaccine adjuvant QS-21, Front. Immunol. 7 (2017) 663, https://doi.org/10.3389/fimmu.2016.00663.
[10] D.J. Marciani, Elucidating the mechanisms of action of saponin-derived adjuvants, Trends Pharmacol. Sci. 39 (2018) 573–585.
[11] F. Kopp, J.T. Mendell, Functional classification and experimental dissection of long noncoding RNAs, Cell 172 (2018) 393–407.
[12] M.K. Atianand, D.R. Caffrey, K.A. Fitzgerald, Immunobiology of long noncoding RNAs, Annu. Rev. Immunol. 35 (2017) 177–198.
[13] Y.G. Chen, A.T. Satpathy, H.Y. Chang, Gene regulation in the immune system by long noncoding RNAs, Nat. Immunol. 18 (2017) 962–972.
[14] M. Krawczyk, B.M. Emerson, p50-associated COX-2 extragenic RNA (PACER) activates COX-2 gene expression by occluding repressive NF-κB complexes, Elife 3 (2014) e01776, https://doi.org/10.7554/eLife. 01776.
[15] Z.H. Li, T.C. Chao, K.Y. Chang, N.W. Lina, V.S. Patila, C. Shimizuc, S.R. Headd, J.C. Burnsc, T.M. Rana, The long noncoding RNA THRIL regulates TNFα expression through its interaction with hnRNPL, Proc. Natl. Acad. Sci. U.S.A. 111 (2014) 1002–1007.
[16] A. Castellanos-Rubio, N. Fernandez-Jimenez, R. Kratchmarov, X. Luo, G. Bhagat, P.H. Green, R. Schneider, M. Kiledjian, J.R. Bilbao, S. Ghosh, A long noncoding RNA associated with susceptibility to celiac disease, Science 352 (2016) 91–95.
[17] S. Carpenter, D. Aiello, M.K. Atianand, E.P. Ricci, P. Gandhi, L.L. Hall, M. Byron, B. Monks, M. Henry-Bezy, J.B. Lawrence, L.A.J. O'Neill, M.J. Moore, D.R. Caffrey, K.A. Fitzgerald, A long noncoding RNA mediates both activation and repression of immune response genes, Science 341 (2013) 789–792.
[18] M.K. Atianand, W. Hu, A.T. Satpathy, Y. Shen, E.P. Ricci, J.R. Alvarez-Dominguez, A. Bhatta, S.A. Schattgen, J.D. McGowan, J. Blin, J.E. Braun, P. Gandhi, M.J. Moore, H.Y. Chang, H.F. Lodish, D.R. Caffrey, K.A. Fitzgerald, A long noncoding RNA lincRNA-EPS acts as a transcriptional brake to restrain inflammation, Cell 165 (2016) 1672–1685.
[19] P. Wang, J.F. Xu, Y.J. Wang, X.T. Cao, An interferon-independent lncRNA promotes viral replication by modulating cellular metabolism, Science 358 (2017) 1051–1055.
[20] M. Du, L. Yuan, X. Tan, D.D. Huang, X.J. Wang, Z. Zheng, X.X. Mao, X.R. Li, L. Yang, K. Huang, F.X. Zhang, Y. Wang, X. Luo, D. Huang, K. Huang, The LPS-inducible lncRNA Mirt2 is a negative regulator of inflammation, Nat. Commun. 8 (2017) 2049–2067.
[21] Y. Zhang, X.T. Cao, Long noncoding RNAs in innate immunity, Cell. Mol. Immunol. 13 (2016) 138–147.
[22] H.X. Sun, S.W. He, M.H. Shi, Adjuvant-active fraction from *Albizia julibrissin* saponins improves immune responses by inducing cytokine and chemokine at the site of injection, Int. Immunopharmacol. 22 (2014) 346–355.
[23] B.N. Zhu, T.Y. He, X.Y. Gao, M.H. Shi, H.X. Sun, Evaluation and characteristics of immunological adjuvant activity of purified fraction of *Albizia julibrissin* saponins, Immunol. Invest. 48 (2019) 283–302.
[24] N.I. Ho, L.G.M. Huis in 't Veld, T.K. Raaijmakers, G.J. Adema, Adjuvants enhancing cross-presentation by dendritic cells: the key to more effective vaccines? Front. Immunol. 9 (2018) 2874, https://doi.org/10.3389/fimmu.2018.02874.
[25] B. Beutler, Innate immunity: an overview, Mol. Immunol. 40 (2004) 845–859.
[26] J.W. Hartley, L.H. Evans, K.Y. Green, Z. Naghashfar, A.R. Macias, P.M. Zerfas, J.M. Ward, Expression of infectious murine leukemia viruses by RAW264.7 cells, a potential complication for studies with a widely used mouse macrophage cell line, Retrovirol. 5 (2008) 1–6.
[27] S.F.G. van Helden, F.N. van Leeuwen, C.G. Figdor, Human and murine model cell lines for dendritic cell biology evaluated, Immunol. Lett. 117 (2008) 191–197.
[28] Y.F. He, T.T. Ni, Z.Y. Liu, Y.P. Ye, H.X. Sun, Rapid annotation and structural characterization of saponins in the active fraction of *Albizia julibrissin* by HPLC coupled with quadrupole time-of-flight mass spectrometry based on accurate mass database, J Sep. Sci. 42 (2019) 2922–2941.
[29] H.X. Sun, J. Zhang, F.Y. Chen, X.F. Chen, Z.H. Zhou, H. Wang, Activation of RAW264.7 macrophages by the polysaccharide from the roots of *Actinidia eriantha* and its molecular mechanisms, Carbohyd. Polym. 121 (2015) 388–402.
[30] X.F. Chen, L.J. Yuan, J. Du, C.Q. Zhang, H.X. Sun, The polysaccharide from the roots of *Actinidia eriantha* activates RAW264.7 macrophages *via* regulating microRNA expression, Int. J. Biol. Macromol. 132 (2019) 203–212.
[31] Q.J. Chen, J. Tao, H.Y. Hei, F.P. Li, Y.M. Wang, W. Peng, X.M. Zhang, Up-regulatory effects of curcumin on large conductance Ca^{2+}-activated K^+ channels, *PloS* One 10 (2015) e0144800, https://doi.org/10.1371/journal.pone.0144800.
[32] J. Du, X.F. Chen, C.Y. Wang, H.X. Sun, Pathway analysis of global gene expression change in dendritic cells induced by the polysaccharide from the roots of *Actinidia eriantha*, J. Ethnopharmacol. 214 (2018) 141–152.
[33] X.F. Chen, J. Du, Y.L. Zhu, C.Q. Zhang, H.X. Sun, Comprehensive analysis of lncRNA and mRNA expression profiles in macrophages activated by *Actinidia eriantha* polysaccharide, Int. J. Biol. Macromol. (2019).
[34] D.W. Huang, B.T. Sherman, R.A. Lempicki, Systematic and integrative analysis of large gene lists using DAVID bioinformatics resources, Nat. Protoc. 4 (2008) 44, https://doi.org/10.1038/nprot.2008.211.
[35] A. Krämer, J. Green, J. Pollard Jr, S. Tugendreich, Causal analysis approaches in ingenuity pathway analysis, Bioinformatics 30 (2014) 523–530.
[36] P.J. Kersey, J.E. Allen, A. Allot, M. Barba, S. Boddu, B.J. Bolt, D. Carvalho-Silva, M. Christensen, P. Davis, C.G.N. Kumar, Z. Liu, T. Maurel, B. Moore, M.D. McDowall, U. Maheswari, G. Naamati, V. Newman, C.K. Ong, M. Paulini, H. Pedro, E. Perry, M. Russell, H. Sparrow, E. Tapanari, K. Taylor, A. Vullo, G. Williams, A. Zadissia, A. Olson, J. Stein, S. Wei, M. Tello-Ruiz, D. Ware, A. Luciani, S. Potter, R.D. Finn, M. Urban, K.E. Hammond-Kosack, D.M. Bolser, N.D. Silva, K.L. Howe, N. Langridge, G. Maslen, D.M. Staines, A. Yates, Ensembl Genomes, An integrated omics infrastructure for non-vertebrate species, Nucleic Acids Res. 46 (2018) (2018) D802–D808.
[37] S.S. Fang, L.L. Zhang, J.C. Guo, Y.W. Niu, Y. Wu, H. Li, L.H. Zhao, X.Y. Li, X.Y. Teng, X.H. Sun, L. Sun, M.H. Zhang, R.S. Chen, Y. Zhao, NONCODEV5: a comprehensive annotation database for long non-coding RNAs, Nucleic Acids Res. 46 (2017) D308–D314.
[38] L. Kong, Y. Zhang, Z.Q. Ye, X.Q. Liu, S.Q. Zhao, L.P. Wei, G. Gao, CPC: assess the protein-coding potential of transcripts using sequence features and support vector machine, Nucleic Acids Res. 35 (2007) W345–W349.
[39] A. Armaos, D. Cirillo, G. Gaetano Tartaglia, omiXcore: a web server for prediction of protein interactions with large RNA, Bioinformatics 33 (2017) 3104–3106.
[40] Z.H. Li, H.J. Ouyang, M. Zheng, B. Cai, P.G. Han, B.A. Abdalla, Q.H. Nie, X.Q. Zhang, Integrated analysis of long non-coding RNAs (lncRNAs) and mRNA expression profiles reveals the potential role of lncRNAs in skeletal muscle development of the chicken, Front. Physiol. 7 (2017) 687, https://doi.org/10.3389/fphys.2016.00687.
[41] S.Y. Wang, X.L. Fan, Q.N. Yu, M.X. Deng, Y.Q. Sun, W.X. Gao, C.L. Li, J.B. Shi, Q.L. Fu, The lncRNAs involved in mouse airway allergic inflammation following induced pluripotent stem cell-mesenchymal stem cell treatment, Stem Cell Res. Ther. 8 (2017) 2, https://doi.org/10.1186/s13287-016-0456-3.
[42] R. Hu, X. Sun, lncRNATargets: A platform for lncRNA target prediction based on nucleic acid thermodynamics, J. Bioinf. Comput. Biol. 14 (2016) 1650016, https://doi.org/10.1142/S0219720016500165.
[43] K.B. Cook, H. Kazan, K. Zuberi, Q. Morris, T.R. Hughes, RBPDB: a database of RNA-binding specificities, Nucleic Acids Res. 39 (2010) D301–D308.
[44] P. Shannon, A. Markiel, O. Ozier, N.S. Baliga, J.T. Wang, D. Ramage, N. Amin, B. Schwikowski, T. Ideker, Cytoscape: a software environment for integrated models of biomolecular interaction networks, Genome Res. 13 (2003) (2003) 2498–2504.
[45] P. Wang, Y.Q. Xue, Y.M. Han, L. Lin, C. Wu, S. Xu, Z.P. Jiang, J.F. Xu, Q.Y. Liu, X.T. Cao, The STAT3-binding long noncoding RNA lnc-DC controls human dendritic cell differentiation, Science 344 (2014) 310–313.
[46] P.J. Murray, J.E. Allen, S.K. Biswas, E.A. Fisher, D.W. Gilroy, S. Goerdt, S. Gordon, J.A. Hamilton, L.B. Ivashkiv, T. Lawrence, M. Locati, A. Mantovani, F.O. Martinez, J. Mege, D.M. Mosser, G. Natoli, J.P. Saeij, J.L. Schultze, K.A. Shirey, A. Sica, J. Suttles, I. Udalova, J.A. van Ginderachter, S.N. Vogel, T.A. Wynn, Macrophage activation and polarization: nomenclature and experimental guidelines, Immunity 41 (2014) 14–20.
[47] M. Kool, T. Soullie, M. van Nimwegen, M.A. Willart, F. Muskens, S. Jung, H.C. Hoogsteden, H. Hammad, B.N. Lambrecht, Alum adjuvant boosts adaptive immunity by inducing uric acid and activating inflammatory dendritic cells, J. Exp. Med. 205 (2008) 869–882.
[48] M. Vono, M. Taccone, P. Caccin, M. Gallotta, G. Donvito, S. Falzoni, E. Palmieri, M. Pallaoro, R. Rappuoli, F.D. Virgilio, E. De Gregorio, C. Montecucco, A. Seubert, The adjuvant MF59 induces ATP release from muscle that potentiates response to vaccination, Proc. Natl. Acad. Sci. U. S. A. 110 (2013) 21095–21100.
[49] S. Musah, N. DeJarnett, G.W. Hoyle, Tumor necrosis factor-α mediates interactions between macrophages and epithelial cells underlying proinflammatory gene expression induced by particulate matter, Toxicol. 299 (2012) 125–132.
[50] T. Nagano, P. Fraser, No-nonsense functions for long noncoding RNAs, Cell 145 (2011) 178–181.
[51] M. Guttman, J.L. Rinn, Modular regulatory principles of large non-coding RNAs, Nature 482 (2012) 339–346.
[52] A.M. Schmitt, H.Y. Chang, Long noncoding RNAs in cancer pathways, Cancer cell 29 (2016) 452–463.
[53] D.M. Anderson, K.M. Anderson, C.L. Chang, C.A. Makarewich, B.R. Nelson, J.R. McAnally, P. Kasaragod, J.M. Shelton, J. Liou, R. Bassel-Duby, E.N. Olson, A micropeptide encoded by a putative long noncoding RNA regulates muscle performance, Cell 160 (2015) 595–606.
[54] K. Schuh, S. Uldrijan, S. Gambaryan, N. Roethlein, L. Neyses, Interaction of the plasma membrane Ca^{2+} pump 4b/CI with the Ca^{2+}/calmodulin-dependent membrane-associated kinase CASK, J. Biol. Chem. 278 (2003) 9778–9783.
[55] J. Li, A. Aderem, MacMARCKS, a novel member of the MARCKS family of protein kinase C substrates, Cell 70 (1992) 791–801.
[56] A.E. Finlayson, K.W. Freeman, A cell motility screen reveals role for MARCKS-

related protein in adherens junction formation and tumorigenesis, PLoS One 4 (2009) e7833, https://doi.org/10.1371/journal.pone.0007833.
[57] M. Fallahi, A.L. Amelio, J.L. Cleveland, R.J. Rounbehler, CREB targets define the gene expression signature of malignancies having reduced levels of the tumor suppressor tristetraproli, PloS One 9 (2014) e115517, https://doi.org/10.1371/journal.pone.0115517.
[58] W.S. Lai, E. Carballo, J.R. Strum, E.A. Kennington, R.S. Phillips, P.J. Blackshear, Evidence that tristetraprolin binds to AU-rich elements and promotes the deadenylation and destabilization of tumor necrosis factor alpha mRNA, Mol. Cell. Biol. 19 (1999) 4311–4323.
[59] P. Briata, D. Bordo, M. Puppo, F. Gorlero, M. Rossi, N. Perrone-Bizzozero, R. Gherzi, Diverse roles of the nucleic acid-binding protein KHSRP in cell differentiation and disease, Wiley Interdiscip. Rev. RNA 7 (2016) 227–240.
[60] N. Peunova, G. Enikolopov, Amplification of calcium-induced gene transcription by nitric oxide in neuronal cells, Nature 364 (1993) 450–453.
[61] A.J. Moreno-Ortega, I. Buendia, L. Mouhid, J. Egea, S. Lucea, A. Ruiz-Nuño, M.G. López, M.F. Cano-Abad, CALHM1 and its polymorphism P86L differentially control Ca^{2+} homeostasis, mitogen-activated protein kinase signaling, and cell vulnerability upon exposure to amyloid β, Aging cell 14 (2015) 1094–1102.